J Mar Sci Technol (2008) 13:256–268
DOI 10.1007/s00773-008-0004-7

ORIGINAL ARTICLE

Hydrodynamic derivatives investigation of unconventionally arranged pusher-barge systems

Koh King Koh · Hironori Yasukawa · Noritaka Hirata

Received: 9 July 2007 / Accepted: 25 December 2007 / Published online: 23 July 2008
JASNAOE 2008

Abstract Unconventional arrangements of pusher-barge systems were studied in this paper. Pusher-barge systems consisting of 4, 6, and 8 barges with one pusher were tested in various combinations. Captive model testing was performed on the various combinations at the Hiroshima University towing tank. Hydrodynamic derivatives of the systems were obtained from the model test data by using the least-square analysis method. For asymmetric conditions, the hydrodynamic derivatives $Y'_0, Y'_{\beta\beta}, N'_0$, and $N'_{\beta\beta}$ were added to the force and moment equations in order to obtain better fitting of the least-square curves. Motion equations were modified to cover the asymmetric cases of pusher-barge systems with lateral force and yaw moment due to the asymmetry arrangement. Turning simulations (with 20° sudden angle change) were carried out and a comparison of advance distance and tactical diameter made.

Keywords Pusher-barge · Unconventional arrangement · Hydrodynamic derivatives · Simulation

1 Introduction

Barge transportation has seen rapid growth in recent years due to the demands of coal mining and transportation. With a relatively spacious design and low operating cost, barges have been the preferred means of transportation for large quantities of cargo. Multiple barges tied together and removed by a pusher have been a popular practice in many countries, including in Asia, such as on the Kapuas River in Kalimantan (Indonesia), the Rejang River in Sarawak (Malaysia), and the Mekong River in Laos. River width restriction is the main concern when choosing a suitable combination for the pusher-barge system.

Nine different combinations of pusher-barge system arranged symmetrically port and starboard have been studied by the authors [1, 2]. Sometimes, pusher-barge systems in the conventional combination might not be favored, due to the cargo type and size, and sea transportation laws of a country. As part of a continuing study of pusher-barge transportation, unconventional arrangements of pusher-barge system were tested at the towing tank at Hiroshima University. Eight different combinations of pusher-barge system were tested, with the pusher located either at the aft or side of the barges. An example of the pusher-barge systems using during model testing is shown in Fig. 1.

2 Pusher-barge system

With reference to Pfenningstorf's paper [3], a pusher with twin screws and twin rudders was designed and tested at the Hiroshima University towing tank, together with various combinations of barges. Two types of barges were designed: rake-barges and box-barges. The rake-barge is always the leading barge, with a rounded bow, and the box-barge is a central or aft barge. Body plans of the pusher and rake-barge are shown in Figs. 2 and 3, and the principal dimensions of the pusher and barges are given in Table 1.

K. K. Koh (✉) · H. Yasukawa · N. Hirata
Graduate School of Engineering, Hiroshima University,
1-4-1 Kagamiyama, Higashi Hiroshima 739-8527, Japan
e-mail: khoking@gmail.com

H. Yasukawa
e-mail: yasukawa@naoe.hiroshima-u.ac.jp

N. Hirata
e-mail: nhirata@naoe.hiroshima-u.ac.jp

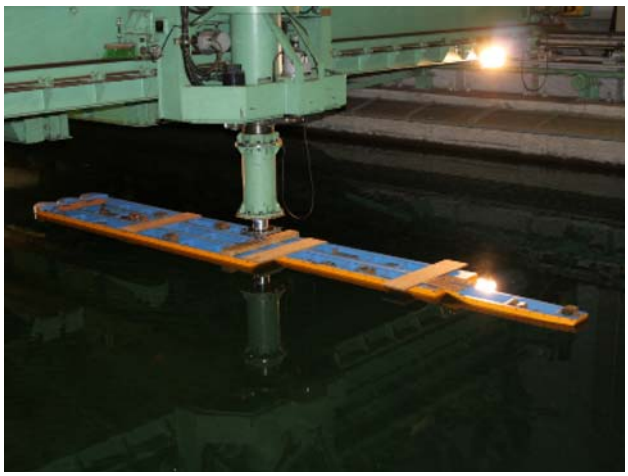

Fig. 1 Pusher-barge 8BP(1) during model testing

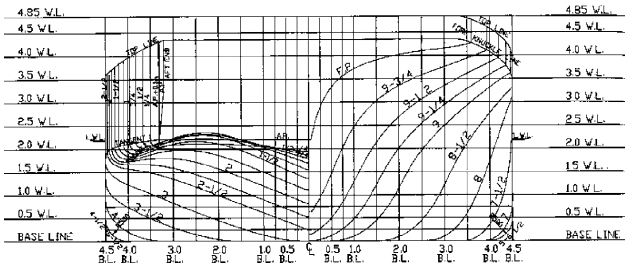

Fig. 2 Body plan of the pusher

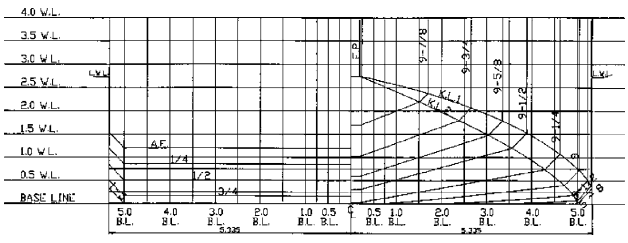

Fig. 3 Body plan of the rake-barge

The designed pusher had two controllable-pitch propellers (CPP) with diameter (D_P) 1.8 m, rotation rate of 300 rpm, and main engine power of 1,340 ps. Rudders used in the pusher had a span of 2.0 m, cord of 2.0 m, and area of 4.0 m^2 each.

Eight different combinations of pusher-barge system were designed. Among them, pusher-barge combinations 4BP(1), 6BP(1), and 6BP(2) are of conventional type and their performance and characteristics have been presented previously [1]. Pusher-barge combinations 4BP(2), 6BP(3), 8BP(1), 8BP(2), and 8BP(3) are new unconventional types, with 8BP(1) and 8BP(2) having an asymmetric port and starboard arrangement. Pusher-barge combinations 4BP(2), 8BP(2), and 8BP(3) have the pusher located between the barges, while the others all have the pusher located at the aft of the system. Figure 4 shows the designation of the various combinations of the pusher-barge systems, and their main characteristics are given in Table 2, wherein LOA is the overall length of the pusher-barge system from the foremost part of the system to the farthest point aft.

3 Hydrodynamic characteristics

3.1 Model test outline

Circular motion testing (CMT) was carried out at Hiroshima University towing tank (100 m length × 7 m width × 4 m depth). Pusher and barge models were built at a scale of 1/50 and each pusher-barge system was tested at the corresponding full-scale speed of 7 knots and draught of 2.74 m. During the testing, the model was restrained from roll and heave motions but free to trim. Force and moment transducers were placed at the midship point of the pusher-barge system (exactly halfway along the pusher barges combination). Longitudinal force (X_H^*), lateral force (Y_H^*), and yawing moment (N_H) were measured and then nondimensionalized by using the following equations:

Table 1 Principal dimensions of the pusher, rake-barge, and box-barge at full and model scale under experiment conditions

	Pusher		Box-barge		Rake-barge	
	Full scale	Model	Full scale	Model	Full scale	Model
Length overall, LOA (m)	40.0	0.80	60.96	1.219	60.96	1.219
Length btw. perpendiculars, LBP (m)	39.50	0.79	60.96	1.219	60.96	1.219
Breadth,B (m)	9.00	0.18	10.67	0.213	10.67	0.213
Draught,d (m)	2.2	0.044	2.74	0.0548	2.74	0.0548
Volume, ∇ (m^3)	494.7	0.00396	1,707.6	0.01366	1,646.2	0.01317
LCB from AP (m)	21.98	0.4395	30.48	0.6096	29.44	0.5888
Block coefficient,C_b	0.633	0.633	0.958	0.958	0.924	0.924

Fig. 4 Pusher-barge systems in eight different combinations

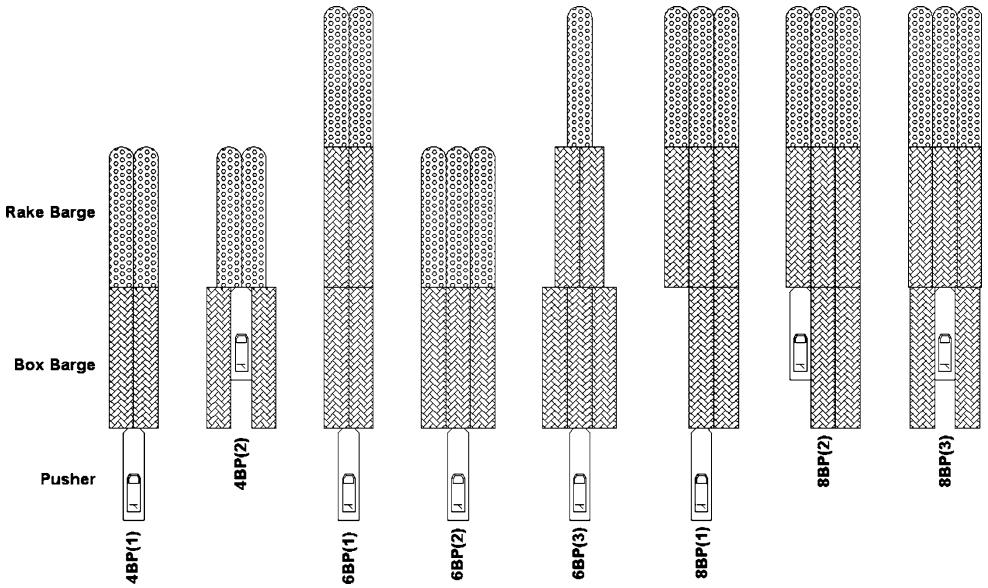

Table 2 Principal dimensions of the pusher-barge systems at full scale

Symbol	4BP(1)	4BP(2)	6BP(1)	6BP(2)	6BP(3)	8BP(1)	8BP(2)	8BP(3)
LOA (m)	161.92	121.92	222.88	161.92	222.88	222.88	182.88	182.88
B (m)	21.34	30.34	21.34	32.01	32.01	32.01	32.01	32.01
d (m)	2.74	2.74	2.74	2.74	2.74	2.74	2.74	2.74
∇ (m^3)	7,202	7,202	10,618	10,556	10,679	13,971	13,971	13,971
LCB from AP (m)	94.54	58.73	125.30	96.24	105.86	133.84	96.00	96.00
C_b	0.761	0.711	0.815	0.743	0.546	0.715	0.871	0.871

$$X'^{*}_H, Y'^{*}_H = \frac{X^{*}_H, Y^{*}_H}{(1/2)\rho\ \mathrm{LOA}\ dU^2}, \tag{1}$$

$$N'_H = \frac{N_H}{(1/2)\rho\ \mathrm{LOA}^2\ dU^2}, \tag{2}$$

where LOA is the overall length of the pusher-barge system, ρ is the water density, d is the draught, and U is the ship speed. Figures 6, 7, and 8 show plots of the nondimensional longitudinal and lateral forces and yawing moment around midship measured during testing of the models. Forces measured in the model tests have the virtual masses of the ship included. A more precise representation of the forces is shown below:

$$X'^{*}_H = X'_H - (m' + m'_y) r' \sin\beta_m, \tag{3}$$

$$Y'^{*}_H = Y'_H - (m' + m'_x) r' \cos\beta_m, \tag{4}$$

where β_m is the drift angle at midship, r' is the nondimensional value of the yaw rate ($r' \equiv r\ \mathrm{LOA}/U$), X'_H and Y'_H are the hydrodynamic forces of the pusher-barge model without the virtual masses of the ship, and m_x, and m_y are the nondimensional mass values with the following definition:

$$m', m'_x, m'_y = \frac{m, m_x, m_y}{(1/2)\rho\ \mathrm{LOA}^2\ d} \tag{5}$$

3.2 Hydrodynamic derivatives: equations evaluation

Hydrodynamic derivatives equations as presented by the authors [1, 2] are good for symmetrically arranged pusher-barge systems (Eq. 6). In order to represent the actual model test data more accurately for asymmetrically arranged pusher-barge systems, four new hydrodynamic derivative terms (Y'_0, $Y'_{\beta\beta}$, N_0, and $N'_{\beta\beta}$) were introduced. The new hydrodynamic derivatives equations are shown in Eq. 7.

$$\left.\begin{aligned} X''_H &= X'_0 \cos^2\beta_m + X'_{\beta\beta}\beta_m^2 + X'_{\beta r}\beta_m r' + X'_{rr} r'^2 \\ Y'_H &= Y'_\beta \beta_m + Y'_r r' + Y'_{\beta\beta\beta}\beta_m^3 + Y'_{\beta\beta r}\beta_m^2 r' \\ N'_H &= N'_\beta \beta_m + N'_r r' + N'_{\beta\beta\beta}\beta_m^3 + N'_{\beta\beta r}\beta_m^2 r' \end{aligned}\right\} \tag{6}$$

$$\left.\begin{aligned} X'_H &= X'_0 \cos^2\beta_m + X'_{\beta\beta}\beta_m^2 + X'_{\beta r}\beta_m r' + X'_{rr} r'^2 \\ Y'_H &= Y'_0 + Y'_\beta \beta_m + Y'_r r' + Y'_{\beta\beta\beta}\beta_m^3 + Y'_{\beta\beta r}\beta_m^2 r' + Y'_{\beta\beta}\beta_m^2 \\ N'_H &= N'_0 + N'_\beta \beta_m + N'_r r' + N'_{\beta\beta\beta}\beta_m^3 + N'_{\beta\beta r}\beta_m^2 r' + N'_{\beta\beta}\beta_m^2 \end{aligned}\right\} \tag{7}$$

In these equations, X'_0 is the forward resistance coefficient, $X'_{\beta\beta}$, $X_{\beta r}$, etc. are the hydrodynamic derivatives on maneuvering. For symmetrically arranged pusher-barge systems, $Y'_0, N'_0, Y'_{\beta\beta}, N'_{\beta\beta}$ are equal to zero. $Y'_{\beta rr}, Y'_{rrr}, N'_{\beta rr}$, and N'_{rrr} were eliminated as in the circular motion tests, at $r' = 0.2$, high accuracy for larger power of r' is hard to achieve [2]. For the pusher-barge arrangements 8BP(1) and 8BP(2), it was found that using Eq. 7 gave better curve fitting to the experiment data. Figure 5 shows a comparison of the asymmetrically arranged pusher-barge systems 8BP(1) and 8BP(2) using Eqs. 6 and 7 for Y'_H, and N'_H curves. From the figure it can be seen that Eq. 7 gives a better fit to the N'_H curves for asymmetrically arranged pusher-barge systems, while the Y'_H curves are similar for both equations.

3.3 Hydrodynamic derivatives: discussion

Resistance coefficient and hydrodynamic derivatives on maneuvering captured from the model tests are shown in Table 3. Figures 6, 7, and 8 show the least-square fitting using Eq. 7 for both symmetrically and asymmetrically arranged pusher-barge systems. The fitting is satisfactory for practical use.

The course stability index, C, is included in Table 3 as well, with the following definition (the rudder effect is not taken into account):

$$C = \frac{N'_r}{Y'_r - m' - m'_x} - \frac{N'_\beta}{Y'_\beta}. \tag{8}$$

From Table 3, it can be seen that pusher-barge combinations 4BP(2), 8BP(2), and 8BP(3) with the pusher located between the barges and are not positioned at the farthest point aft of the system, have negative values of C, which means that they are unstable in course keeping.

4 Added mass coefficients

In this paper, added mass coefficients were calculated using the singularity distribution method under the assumption of a rigid free surface. The designation m_{ij} was used, where

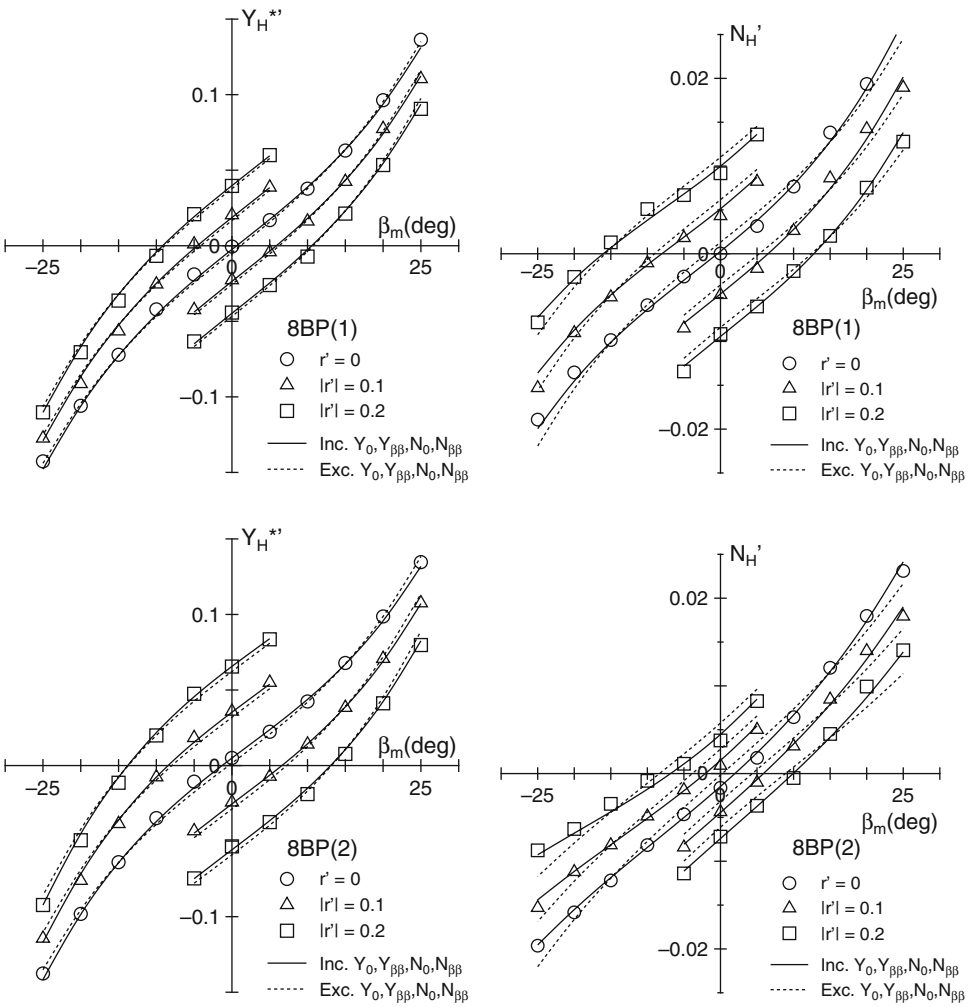

Fig. 5 Fitting comparison of $Y_H^{*\prime}$ and N'_H for the 8BP(1) and 8BP(2) combinations with and without Y_0, $Y'_{\beta\beta}$, N_0, $N'_{\beta\beta}$

Table 3 Resistance coefÞcient, hydrodynamic derivatives on maneuvering, and course stability index

Symbol	4BP(1)	4BP(2)	6BP(1)	6BP(2)	6BP(3)	8BP(1)	8BP(2)	8BP(3)
X'_0	−0.0642	−0.1049	−0.0566	−0.0858	−0.0763	−0.0765	−0.0846	−0.0850
$X'_{\beta\beta}$	−0.0609	−0.1074	−0.0856	−0.0661	−0.0928	−0.0934	−0.0982	−0.1337
X'_{rr}	−0.0085	0.0124	0.0446	0.1128	−0.0064	0.0443	−0.0538	0.0293
$X_{\beta r}-m'_y$	−0.1130	−0.2032	−0.0789	−0.1004	−0.0961	−0.0898	−0.1302	−0.1541
Y'_0	0.0	0.0	0.0	0.0	0.0	−0.0024	0.0050	0.0
Y'_β	0.2544	0.3292	0.2190	0.2442	0.2371	0.2272	0.2161	0.2519
$Y'_r-m'_x$	0.0122	0.0354	−0.0477	0.0137	0.0098	−0.0060	0.0016	0.0130
$Y'_{\beta\beta\beta}$	0.2795	0.7592	0.4809	0.4957	0.4972	0.4857	0.5105	0.6269
$Y'_{\beta\beta r}$	−0.0777	0.4937	−0.4078	0.1332	0.1064	0.1240	0.2993	0.4497
$Y'_{\beta\beta}$	0.0	0.0	0.0	0.0	0.0	−0.0309	−0.0517	0.0
N'_0	0.0	0.0	0.0	0.0	0.0	0.0003	−0.0015	0.0
N'_β	0.0397	0.0561	0.0308	0.0517	0.0298	0.0384	0.0420	0.0338
N'_r	−0.0497	−0.0297	−0.0422	−0.0756	−0.0214	−0.0485	−0.0297	−0.0319
$N'_{\beta\beta\beta}$	0.1381	0.0149	0.1291	0.1137	0.0769	0.0779	0.0424	−0.0020
$N'_{\beta\beta r}$	−0.0789	−0.5045	−0.1791	−0.0989	−0.1045	−0.0785	−0.1140	−0.1753
$N'_{\beta\beta}$	0.0	0.0	0.0	0.0	0.0	0.0158	0.0198	0.0
C	0.1079	−0.0769	0.0663	0.0578	0.0197	0.0607	−0.0964	−0.0247

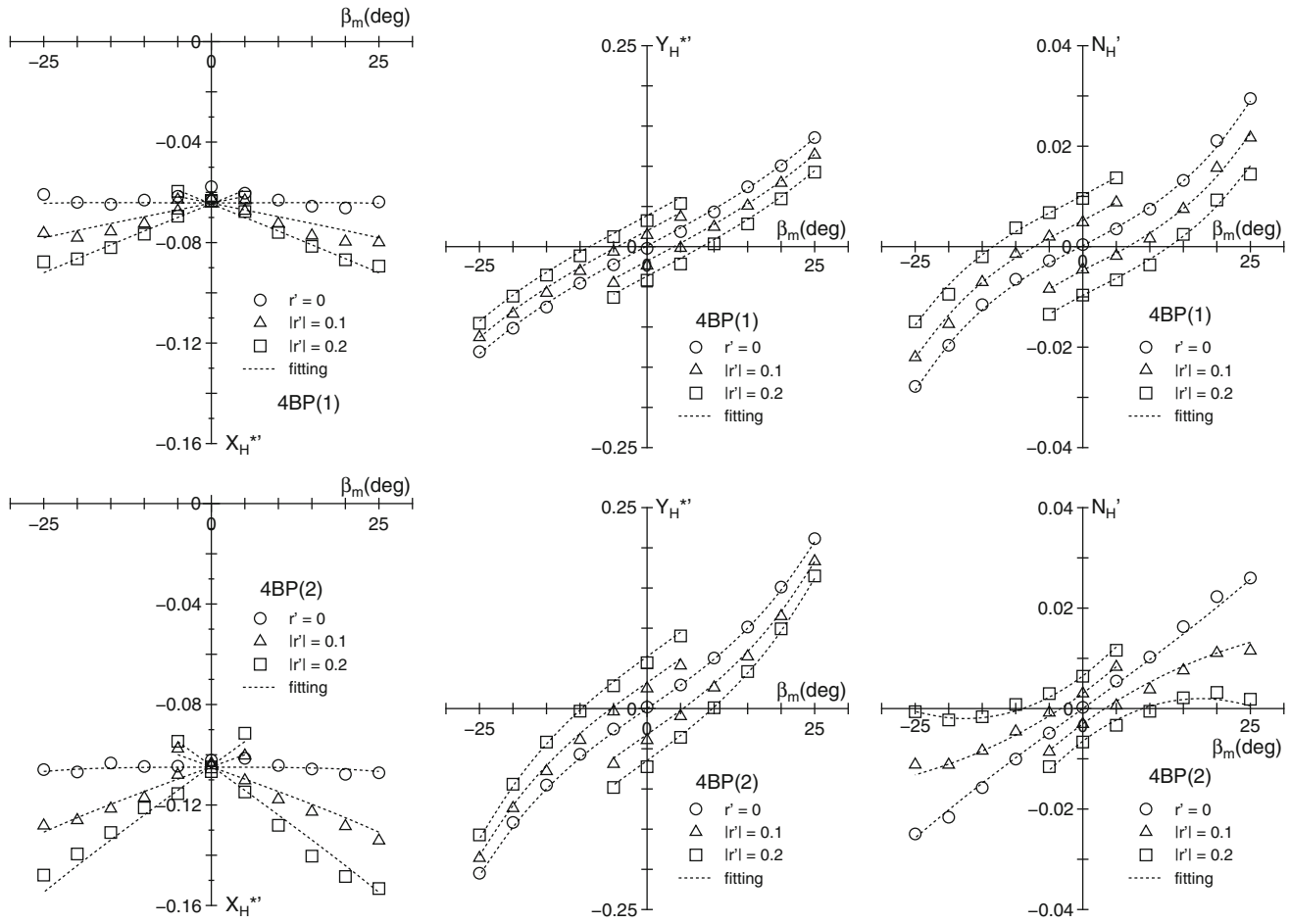

Fig. 6 Measured force and moment coefÞcients for 4BP(1) and 4BP(2)

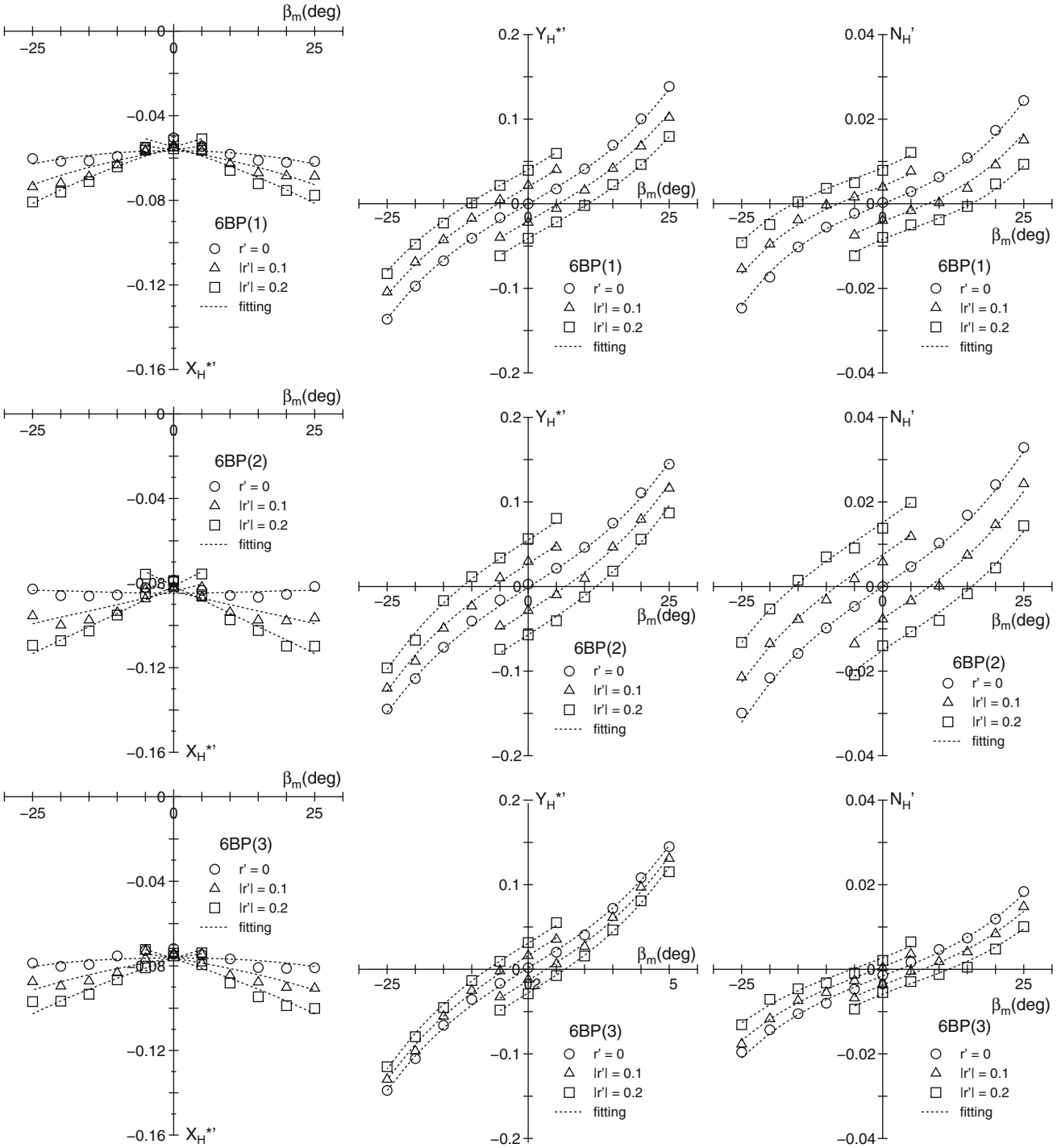

Fig. 7 Measured force and moment coefficients for 6BP(1), 6BP(2), and 6BP(3)

represents the direction and j is the motion mode of a specific added mass: $j = 1$ for surging motion, $j = 2$ for swaying motion, $j = 6$ for yawing motion. m'_{11}, m'_{22}, and m'_{66} represent m'_x, m'_y, and J'_{zz}. Table 4 shows the value of the added mass coefficients for all eight of the pusher-barge systems. For the symmetrically arranged pusher-barge systems, m'_{12} and m'_{16} are equal to zero. For the asymmetrically arranged pusher-barge systems, the effect of uneven lateral force and yaw moment needs to be taken into account in the added mass. The maneuvering simulation described herein includes all the added mass coefficients.

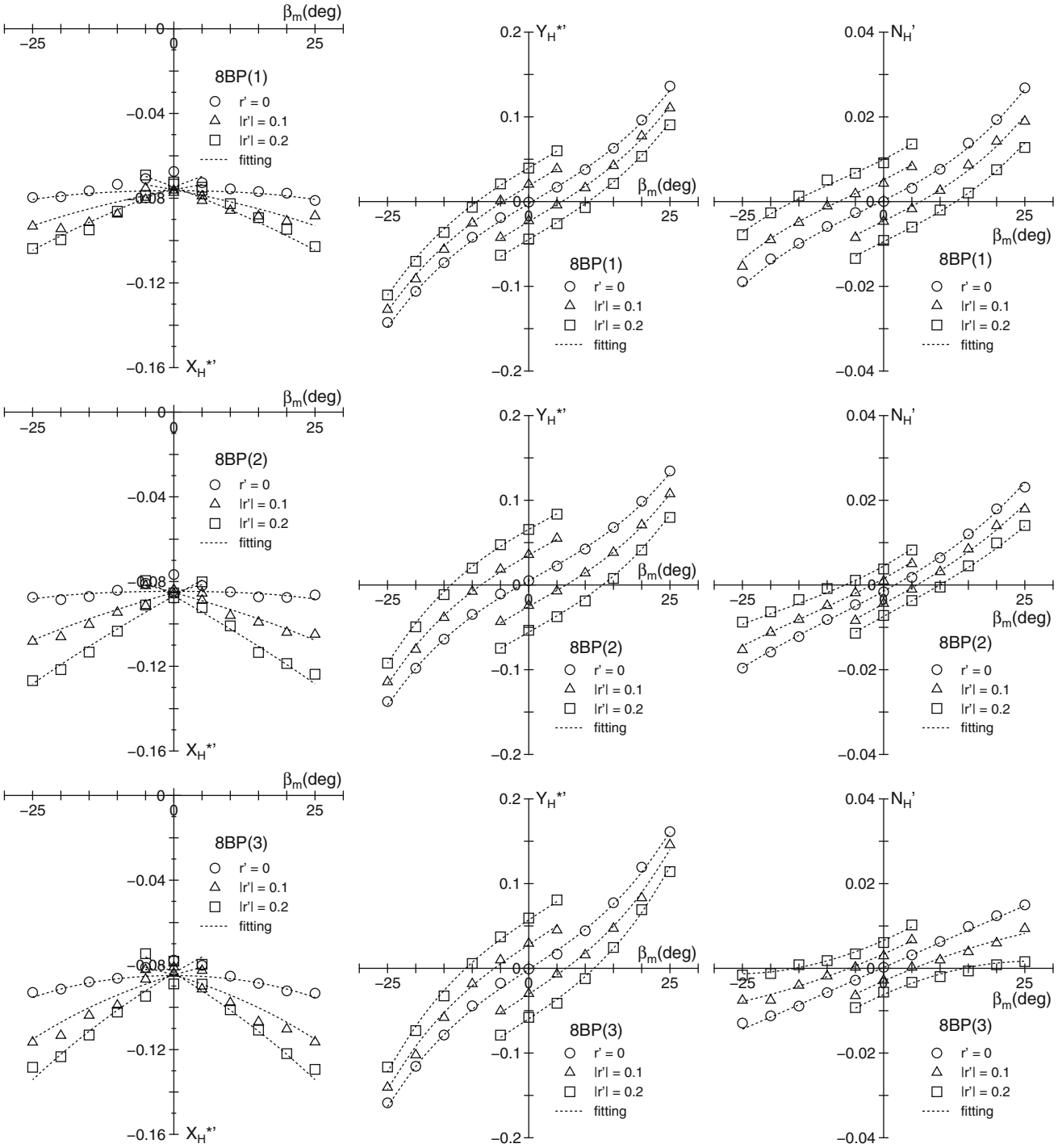

Fig. 8 Measured force and moment coefÞcients for 8BP(1), 8BP(2), and 8BP(3)

5 Effective power

The full-scale effective power of the pusher-barge system was calculated based on the model test total resistance at a ship speed of 7 knots, and the frictional resistance was calculated using the ITTC-1957 formula. Figure 9 shows the residual resistance coefÞcient based on the wetted surface area, the effective power, and the effective power per unit barge of the various pusher-barge combinations. From the Þgures, the following Þndings can be concluded:

- Pusher-barge combinations 4BP(2) and 6BP(3) with extended breadth in the middle and aft caused much higher residual resistance and required higher power to run at a ship speed of 7 knots in their respective series.

Table 4 Added mass coefficients

Symbol	4BP(1)	4BP(2)	6BP(1)	6BP(2)	6BP(3)	8BP(1)	8BP(2)	8BP(3)
m'_x (m'_x)	0.00760	0.01760	0.00437	0.01300	0.00589	0.00685	0.01064	0.01025
m'_y (m'_y)	0.07410	0.14040	0.05740	0.07870	0.05594	0.05984	0.08183	0.09414
m'_{66} (J'_{zz})	0.00430	0.01050	0.00363	0.00446	0.00364	0.00385	0.00610	0.00793
m'_{26}	−0.00127	−0.00542	−0.00069	−0.00175	0.00330	−0.00251	−0.00145	−0.00609
m'_{12}	0.0	0.0	0.0	0.0	0.0	0.00048	0.00104	0.0
m'_{16}	0.0	0.0	0.0	0.0	0.0	−0.00003	−0.00035	0.0

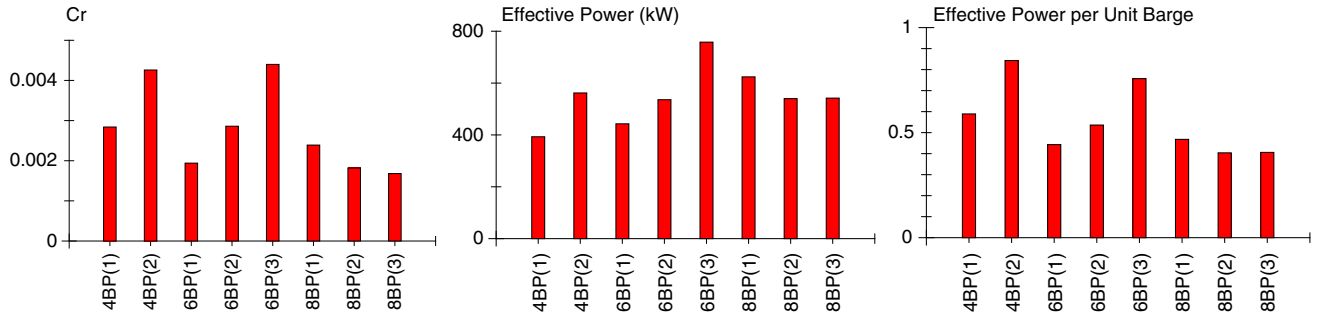

Fig. 9 Comparison of residual resistance coefficient, effective power, and effective power per unit barge (7 knots)

- Pusher-barge combination 8BP(1) with the pusher located farthest aft in the system (longest LOA) had a higher resistance compared with the 8BP(2) and 8BP(3) combinations, in which the pusher is located in-between and at the side of the barges.

To study the effect of the pusher in the pusher-barge system with regards to residual resistance, a simple series of experiments was performed, as described in Appendix A. From these experiments, it can be seen that, by adding a pusher to the aft of a system, residual resistance was increased. Comparison of pusher-barge combination 8BP(1) and 8BP(2) also shows that, by shortening the overall length of the pusher-barge system by moving the location of the pusher to the side of the system, the residual resistance and required horse power to move the system at a constant speed of 7 knots decreased. However, comparison of the 4BP(1) and 4BP(2) combinations reminds us that, if extended breadth is present along the length of the barges, this blocks the water from flowing smoothly and residual resistance can increase dramatically.

In the effective power comparison, for pusher-barge systems that have the same number of barges, the required effective power can be summarized as: 4BP(1) < 4BP(2), 6BP(1) < 6BP(2) < 6BP(3), 8BP(1) > 8BP(2) ≃ 8BP(3). Pusher-barge combinations 8BP(2) and 8BP(3) required similar amounts of power to move at a ship speed of 7 knots, and had the most efficient effective power per unit barge among all the eight pusher-barge systems tested.

6 Maneuvering simulations

6.1 Outline

Maneuvering motions of the pusher-barge systems were simulated using a FORTRAN program written by the authors. The rudder angle used in the simulations was 20°. The effect of wind, waves, and current as well as shallow and restricted water effects were not taken into account in the simulations. Propeller revolution was set at 300 rpm and the initial forward speed of the pusher-barge system was set at 7 knots. In order to maintain a constant forward speed of 7 knots, controllable-pitch propellers (CPP) were used in the simulation. Twin screws and twin rudders were installed at the port and starboard at the aft of the pusher. Each pusher-barge system had its own propeller pitch ratio in order to maintain a constant forward speed of 7 knots at a rudder angle of 0°, but for the asymmetrically arranged pusher-barge systems 8BP(1) and 8BP(2), maintenance of a straight course at constant speed was not achievable without the assistance of rudder control, due to the uneven force in the system. Autopilot was added to the simulation program for these two cases, and it was found that an offset rudder angle of −0.6° (port) was needed for 8BP(1) and 3.7° (starboard) for 8BP(2) to maintain a straight course at a ship speed of 7 knots.

Hydrodynamic derivatives captured from the model tests, as shown in Table 4, were used in the simulation. Details of the calculations used in the simulations are given

Table 5 Propeller, rudder, and hull interaction parameters

Symbol	Value	Symbol	Value
t	0.164	a_H	0.194
w_{P0}	0.34	t_R	0.055
ε	0.987	γ_R	0.23

in Appendix B. Propeller, rudder, and hull interaction parameters used in the simulations, referred to [4], are shown in Table 5.

6.2 Simulations results

Figure 10 shows the turning trajectories of the eight pusher-barge systems with a 20° rudder angle. For the pusher-barge 8BP series, simulations of port and starboard turns are included. For the symmetrically arranged pusher-barge systems, only a starboard turn simulation was carried out, except for 8BP(3) for comparison purposes with the other 8BP series. Figure 11 shows plots of the advance distance and tactical diameter.

In the 4BP series, it was found that, when the pusher was located between the barges (4BP(2)), the tactical diameter and advance distance were reduced by a significant amount. The course stability index, C, does not give much information about the turning behavior of the 4BP series of the pusher-barge system. When further studying the differences in turning performance as related to the various hydrodynamic derivatives, the authors found that some of the nonlinear derivative terms play important roles in influencing the turning performance of the pusher-barge system. They are $Y'_{\beta\beta\beta}$, $Y'_{\beta\beta r}$ and $N'_{\beta\beta r}$. Pusher-barge combination 4BP(2) exhibited a significant increment in these nonlinear hydrodynamic derivatives, which have a high damping effect in turning and should lead to a larger turning circle for 4BP(2). However, the results were otherwise. Hence, the authors checked the rudder force of the 4BP series and found that 4BP(2) had a much higher rudder force difference than 4BP(1) (Fig. 12). This higher

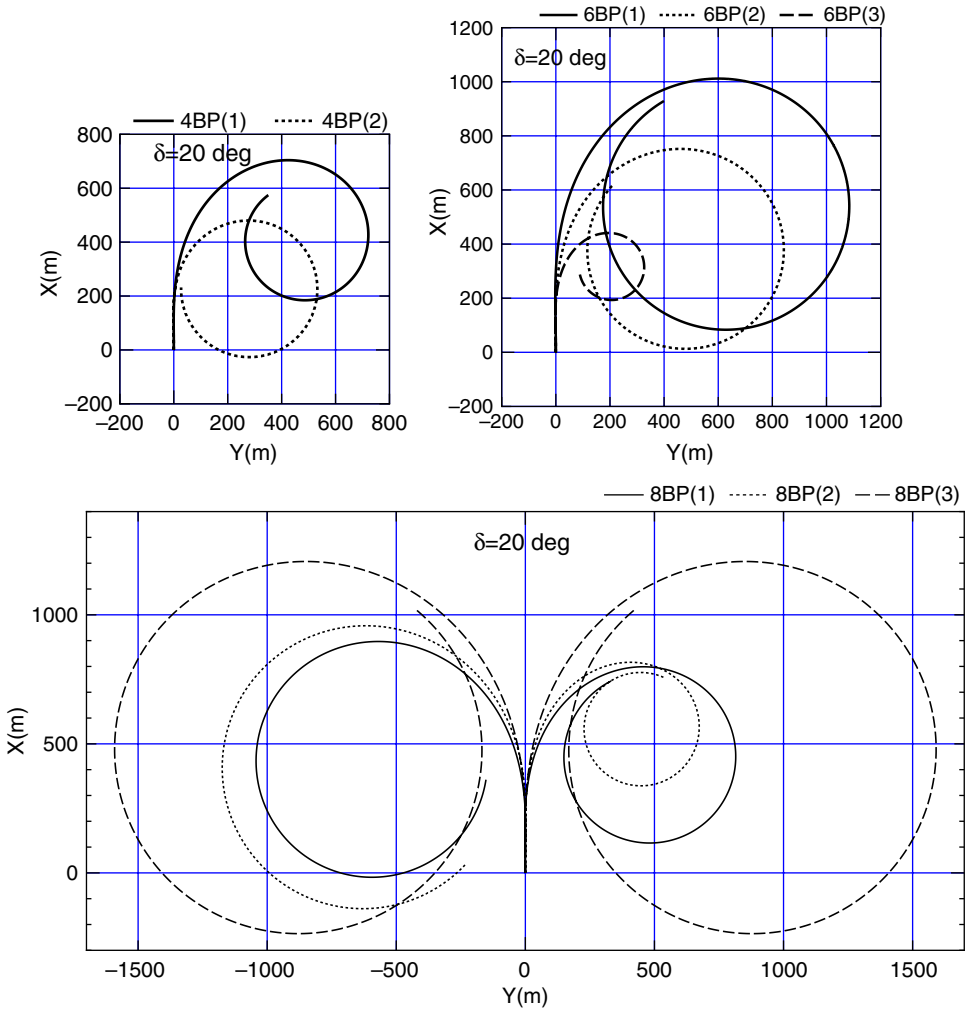

Fig. 10 Turning trajectories (δ = 20°)

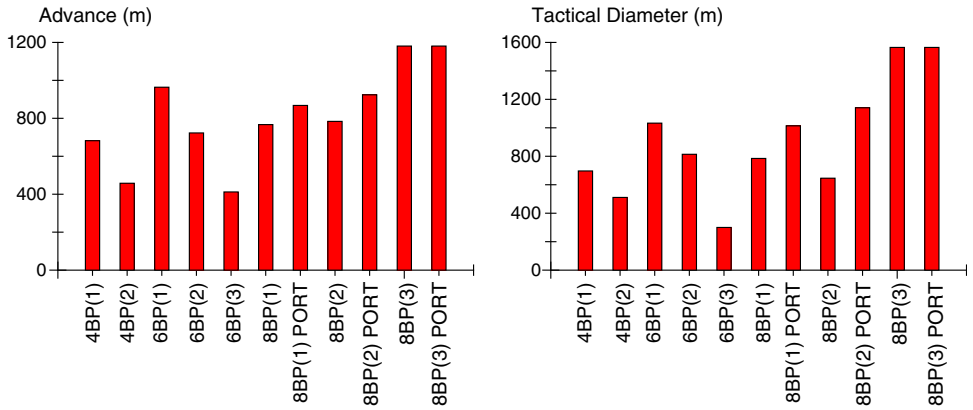

Fig. 11 Tactical diameter and advance distance (δ = 20°)

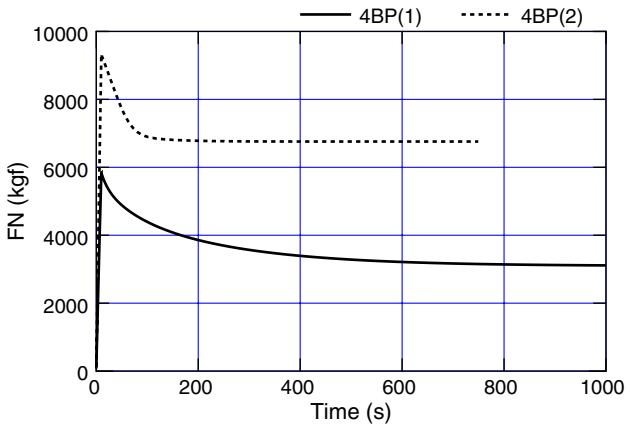

Fig. 12 Rudder force in the 4BP series

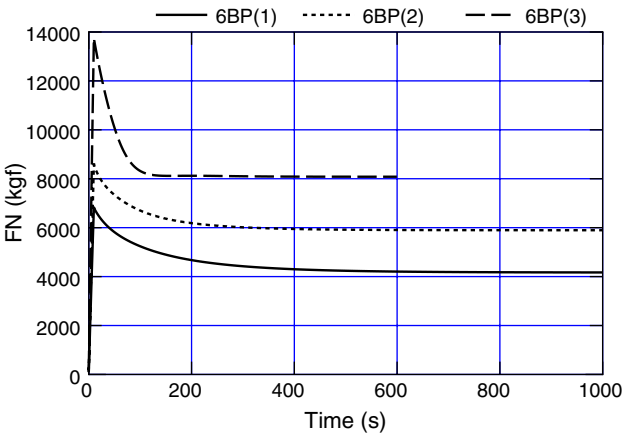

Fig. 13 Rudder force in the 6BP series

rudder force was the reason for the smaller turning circle for 4BP(2), which cancelled out the large damping effect due to the nonlinear hydrodynamic derivatives for the 4BP(2) combination.

In the 6BP series, 6BP(3) with a triangle type of arrangement gave the smallest value for the tactical diameter and advance distance. The course stability index, C, plays an important role in indicating the turning performance of the systems in the 6BP series; the smaller the value of C, the better the turning performance (the smaller the turning circle). The combination 6BP(3) have the smallest value of C, followed by 6BP(2) and then 6BP(3). Another factor that contributes to the smaller turning trajectory of the pusher-barge combination 6BP(3) is its relatively high resistance and the high pitch ratio that directly resulted in high rudder force in pusher-barge 6BP(3) as compared with 6BP(2) and 6BP(1). The large rudder force in 6BP(3) caused turning of 6BP(3) to be much more efficient than the rest. A comparison of the rudder force in the 6BP series is shown in Fig. 13.

In analyzing the results of the 8BP series, the authors took pusher-barge 33BP from [11] to compare with 8BP(1) due to their similar arrangements. A plot comparing the two systems is shown in Fig. 14. From the figure, it is found that pusher-barge 8BP(1) has a very similar turning trajectory to 33BP for port-side turning. This finding matches well with the straight-course moving test conducted by the authors earlier in the simulations when finding the pitch ratio of 8BP(1), where the rudder offset of 8BP(1) is minor (0.6° to port), showing that the asymmetry effect of pusher-barge 8BP(1) is very small. In starboard-side turning, the asymmetry effect has a stronger influence by significantly reducing the turning trajectory. In pusher-barge combination 8BP(2), due to the stronger asymmetry effect (rudder offset of 3.7° to starboard in the straight-course moving test), the pusher-barge combination 8BP(2) has a larger port-side turning trajectory and smaller

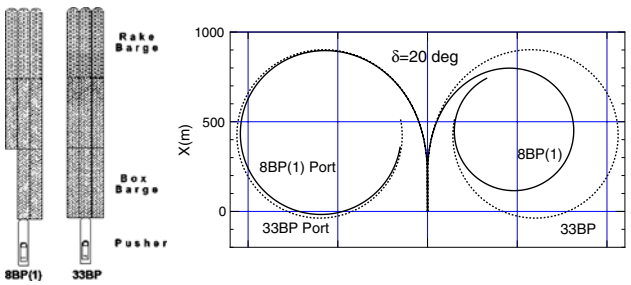

Fig. 14 Turning trajectories of 8BP(1) and 33BP [12]

starboard side turning trajectory than the pusher-barge combination 8BP(1). The turning trajectory of pusher-barge 8BP(3) increased significantly compared with 8BP(1) and 8BP(2). The course stability index, C, does not give much information about the differences in the turning trajectories in the 8BP series, hence analysis was shifted to the individual hydrodynamic derivatives of the various pusher-barge systems. In the 8BP series, the authors found that, for pusher-barge 8BP(3), the nonlinear derivatives $Y'_{\beta\beta\beta}$, $Y'_{\beta\beta r}$ and $N'_{\beta\beta r}$ increased significantly. These nonlinear derivatives have a high damping effect in turning motion, which is the main cause of the significant increase in the turning trajectory of the pusher-barge combination 8BP(3).

Asymmetric arrangement of the pusher-barge systems resulted in an asymmetric hull force for the port and starboard sides. In asymmetric cases, when the arrangement is weighted on one side, the system tends to exhibit a larger turning trajectory on the opposite side, and vice versa. Thus, pusher-barges 8BP(1) and 8BP(2) produce different port and starboard turning trajectories.

7 Concluding remarks

Model experiments of eight different pusher-barge systems were carried out in the Hiroshima University towing tank. Hydrodynamic derivatives were obtained from the experiment data and computer simulation was performed based on the obtained hydrodynamic derivatives. Y'_0, $Y'_{\beta\beta}$, N'_0, and $N'_{\beta\beta}$ were added to the force and moment equations in order to fit the model test data more accurately for the asymmetrically arranged pusher-barge systems. Pusher-barge systems with the pusher located between the barges and not at the farthest point aft of the system (4BP(2), 8BP(2) and 8BP(3)) are unstable in course keeping (negative course stability index, C). Pusher-barge systems with the pusher located between the barges (8BP(2) and 8BP(3)) exhibited lower residual resistance and required less power to operate at a ship speed of 7 knots as compared with 8BP(1). Pusher-barge 4BP(2) on the other hand exhibited a higher resistance compared with 4BP(1) due to the extension of the width in the middle of the system. A similar effect happened with pusher-barge 6BP(3). Breadth extension in the middle of a pusher-barge system should be avoided.

In the computer simulations, uneven force on the port and starboard sides was taken into consideration when calculating the added mass and the total moment of the pusher-barge system. The rudder force and the nonlinear hydrodynamic derivatives ($Y'_{\beta\beta\beta}$, $Y'_{\beta\beta r}$ and $N'_{\beta\beta r}$) play important roles in influencing the turning trajectory of a pusher-barge system. In some cases, the course stability index (C) gives good information about the turning performance, where a smaller value of C indicates better turning performance. For asymmetrically arranged pusher-barge systems, a pusher-barge combination weighted on one side will have a larger turning trajectory when making an opposite turn. Asymmetrically arranged pusher-barge systems will also have different port and starboard turning performance, due to the asymmetry propeller and rudder forces (8BP(2)) and asymmetry hull force (8BP(1) and 8BP(2)).

For future work, the authors suggest conducting captive model testing to capture the value of the propeller, rudder, and hull interaction parameters (current values are based on assumptions). Full-scale test data would also be useful and would allow comparison with simulation results to be performed.

Appendix A: effect of the pusher on the overall pusher-barge system's resistance

Figure 15 shows a comparison of the resistance of four different pusher-barge systems (with and without a pusher). Pusher-barge 1B is to be compared with 1BP, and pusher-barge 2B is to be compared with 2BP. The combinations were tested in the Hiroshima University towing tank at a ship speed of 7 knots, with frictional resistance calculated using the ITTC 1957 formula to obtain the residual resistance. Comparison of the residual resistance coefficient (C_r) based on wetted surface area is plotted in Fig. 16. From the figure, it is found that, by having the pusher at the back of the barges, the residual resistance increased by around 20–25%.

Appendix B: maneuvering motion simulation for asymmetrically arranged pusher-barge system

Figure 17 shows the coordinate systems used herein. O-$X_0Y_0Z_0$ are the space coordinate system, with X_0Y_0

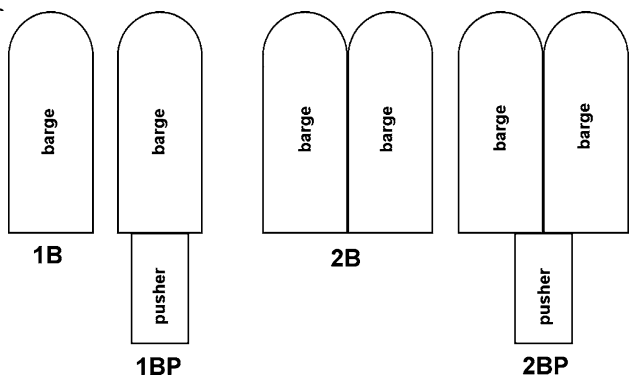

Fig. 15 Pusher-barge systems with and without pusher

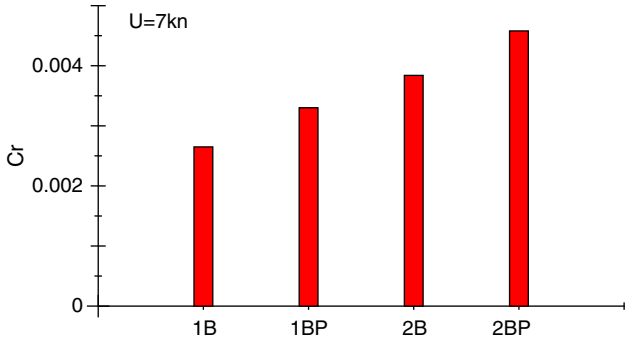

Fig. 16 Residual resistance coefficient comparison

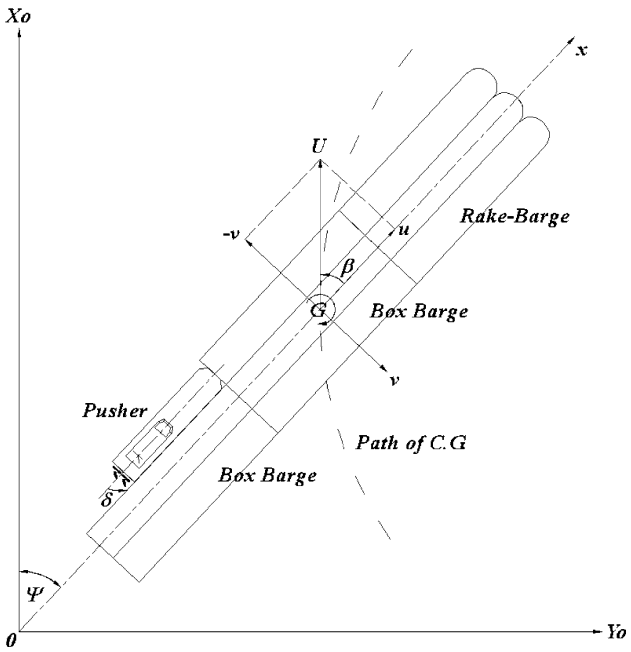

Fig. 17 Coordinate systems

referring to the water surface and Z_0 vertically downwards from the water surface. ψ is the angle from X_0 to the position of the ship. $G-xyz$ is the ship's coordinate system, where G is the center of gravity of the ship, x is the forward direction of the ship, and y is the lateral direction of the ship. The xy plane forms the water surface where the ship is located, and z is the vertical downwards direction from the center of gravity of the ship. Maneuvering motions of the pusher-barge system (surge, sway, and yaw) are defined by the motion equations in Eq. 9, where u is the forward speed, v is the lateral speed, r is the turning rate, m is the mass of the ship, and I_{zz} is the moment of inertia of the ship. m_{ij} $(i = 1, 2, 6; j = 1, 2, 6)$ is the added mass and added moment of inertia of the pusher-barge system that occur when a ship accelerates or decelerates or is in turning motion. On the right-hand side of the equations, X is the total forward force, Y is the total lateral force, and N is the total moment at the center of gravity of the pusher-barge system.

$$\left.\begin{aligned}(m+m_{11})\dot{u}-(m+m_{22})vr+m_{12}\dot{v}+m_{16}\dot{r}&=X\\(m+m_{11})ur+(m+m_{22})\dot{v}+m_{12}\dot{u}+m_{26}\dot{r}&=Y\\(I_{zz}+m_{66})\dot{r}+m_{16}\dot{u}+m_{26}\dot{v}&=N\end{aligned}\right\} \quad (9)$$

X, Y, and N are the forces and moment introduced by the hull (H), propeller (P), and rudder (R), which are expressed in Eq. 10.

$$\left.\begin{aligned}X&=X_H+X_P+X_R\\Y&=Y_H+Y_R\\N&=N_H+N_R-(Y_H+Y_R)x_G-X_Py_P-X_Ry_R\end{aligned}\right\}. \quad (10)$$

In model tank testing, measurement was done at the midship of the pusher-barge system, while the longitudinal force X is unaffected, but the lateral force Y and the moment N must be corrected from midship to the center of gravity of the pusher-barge system. The relationship of the lateral velocity at midship v_m to the lateral velocity at the center of gravity of the pusher-barge system v is given in Eq. 11. The midship drift angle β_m is defined in Eq. 12.

$$v_m = v - x_G r \quad (11)$$

$$\beta_m = \tan^{-1}\left(\frac{-v_m}{u}\right). \quad (12)$$

The hydrodynamic force that acts on a hull when a ship makes a diagonal turn is mainly caused by the dynamic pressure of the fluid. If the flow along the hull is to be related to the ship's length, and the displacement of the hull is to be related to the draught of the ship, then the relationship between the flow and pressure can be related to LOA $\times$ d. The hydrodynamic force (X_H, Y_H, N_H) on a ship's hull based on the above consideration is shown in Eq. 13, where U is the ship's speed ($U = \sqrt{u^2+v^2}$), and X'_H, Y'_H, and N'_H are defined in Eq. 7.

$$\left.\begin{aligned}X_H&=(1/2)\rho\ \mathrm{LOA}\ dU^2X'_H(\beta_m, r')\\Y_H&=(1/2)\rho\ \mathrm{LOA}\ dU^2Y'_H(\beta_m, r')\\N_H&=(1/2)\rho\ \mathrm{LOA}^2\ dU^2N'_H(\beta_m, r')\end{aligned}\right\} \quad (13)$$

The propeller of a ship is assumed to be fixed aft and to only contribute force in the X direction. The total force produced by a propeller as experienced by the ship is defined as:

$$X_P = (1-t)\sum T, \quad (14)$$

where t is the thrust deduction factor and $\sum T$ is the total thrust produced by the propellers (the twin screws in this study).

$$T = \rho n_P^2 D_P^4 K_T(J_P, p) \quad (15)$$

In Eq. 15 D_P is the propeller diameter, K_T is the thrust coefficient, J_P is the propeller advanced coefficient, and

p is the propeller pitch ratio. K_T and J_P are defined in Eqs. 16 and 17.

$$K_T(J_P, p) = -0.3260pJ_P - 0.2005J_P + 0.5234p - 0.0398 \quad (16)$$

$$J_P = \frac{u(1-w_P)}{n_P D_P} \quad (17)$$

In Eq. 17, w_P is the propeller wake fraction factor, which changes according to the drift angle β and also the ship turning rate r'. Hirano's formula [5] was used in calculating the wake fraction factor.

$$w_P = w_{P0}\exp[C_1\beta_P^2], \quad (18)$$

where w_{P0} is the wake factor during forward motion of the pusher-barge system, β_P is the drift angle at the propeller position ($\equiv \beta - \ell'_P r'$), and C_1 is the correction factor. ℓ'_P is the ratio of the position of the propeller location relative to the center of gravity of the pusher-barge system (with forward being positive) to the overall length of the pusher-barge system.

The rudder forces (X_R and Y_R) and moment (N_R) are defined in Eq. 19.

$$\left.\begin{aligned} X_R &= -(1-t_R)\sum F_N \sin\delta \\ Y_R &= -(1+a_H)\sum F_N \cos\delta \\ N_R &= -(x_R + a_H x_H)\sum F_N \cos\delta \end{aligned}\right\} \quad (19)$$

where δ is the rudder angle, t_R, a_H, and x_H are the rudder and hull interaction parameters, and x_R is the x-coordinate point on which the rudder force Y_R acts. x_H is assumed to be $0.85x_R$. F_N is defined as

$$F_N = \frac{1}{2}\rho A_R U_R^2 f_\alpha \sin\alpha_R, \quad (20)$$

where A_R is the rudder area and f_α is the gradient of the lift coefficient of the rudder. f_α is estimated using Fujii's formula [6]. U_R is the flow velocity to the rudder and α_R is the effective rudder in-flow angle:

$$U_R = \sqrt{u_R^2 + v_R^2} \quad (21)$$

$$\alpha_R = \delta - \tan^{-1}\left(\frac{v_R}{u_R}\right) \quad (22)$$

In Eq. 21, u_R is the water flow speed towards the rudder and v_R is the lateral flow speed after passing the propeller. v_R is calculated using Eq. 23, which is related to the rudder location and is influenced by the flow entrance angle to the rudder (β_R ($\equiv \beta - \ell'_R r'$), and γ_R is the flow-rectification coefficient for the rudder. ℓ'_R is the ratio of the effective rudder position relative to the center of gravity of the pusher-barge system (with the forward direction being positive) to the overall length of the pusher-barge system. γ_R is assumed to be $x_R/2$.

$$v_R = U\gamma_R\beta_R \quad (23)$$

u_R is defined using Yoshimura's formula [7] as [

$$u_R = \frac{\varepsilon u_P}{1-s}\sqrt{1 - 2(1-\eta\kappa)s + 1 - \eta\kappa(2-\kappa)s^2}, \quad (24)$$

where s is the propeller slip ratio, η is the ratio of propeller diameter to rudder height, κ is the propeller flow correction factor ($\kappa = 0.6$ is normally used), and ε is the flow coefficient of the rudder with respect to its location.

References

1. Koh KK, Yasukawa H, Hirata N, Kose K (2008) Maneuvering simulations of pusher-barge systems. J Mar Sci Tech 13:117–126
2. Yasukawa H, Hirata N, Koh KK, Punayangkool K, Kose K (2007) Hydrodynamic force characteristics on maneuvering of pusher-barge systems (in Japanese). J Jpn Soc Nav Archit Ocean Eng 5:133–142
3. Pfennigstorf J (1970) Handbuch der Werften X Band. Bearb von K Wendel. Schiffahrts-Verlag HANSA, C Schroedter & Co, Hamburg 11
4. Yoshimura Y, Sakurai H (1989) Mathematical model for the manoeuvring ship motion in shallow water (3rd Report) (in Japanese). J Kansai Soc Nav Archit Jpn 211
5. Hirano M (1980) On the calculation method of ship maneuvering motion at the initial design phase (in Japanese). J Soc Nav Archit Jpn 147:144–153
6. Fujii H, Tuda T (1961) Experimental research on rudder performance (2) (in Japanese). J Soc Nav Archit Jpn 110:31–42
7. Yoshimura Y, Nomoto K (1978) Modeling of maneuvering behaviour of ships with a propeller idling, boosting and reversing (in Japanese). J Soc Nav Archit Jpn 144:57–69